

## APPENDIX

### 1.1 Analytic modeling for extraordinary stiffness tunability

This section follows chapter 6 and provides an analytic derivation to explain the tunable stiffness phenomena. The analysis was done primarily by Marc Serra-Garcia and demonstrates the broader applicability of this concept to other 1-D lattices.

The system considered in chapter 6 consists of a chain of particles coupled through an anharmonic interaction potential (Fig A.1a). In order to get exact results, the motion of all particles needs to be accounted for. However, studying the dynamics of a large number of particles analytically is a difficult problem. In our system we can avoid this complexity by realizing that most of the motion is concentrated around the defect. This is a consequence of the defect mode being highly localized. This localization allows us to capture all of the essential dynamics of the system by considering a single oscillating particle and assuming that other particles in the lattice displace only quasi-statically (Fig A.1c,d). By using this simplification, we can qualitatively reproduce all of the effects that we have observed experimentally, such as the tuned force-displacement relationship of the lattice. In order to accomplish this, we consider the system at a prescribed total displacement, and then proceed to calculate the amplitude of vibration of the defect, as well as the static force at the boundary.

At each fixed compression value, we model the defect as a point mass  $M$ , with a dynamic displacement from equilibrium,  $u_d$ . The defect is subject to a linear damping  $F_d = -b\dot{u}_d$  and a periodic excitation force  $F(t) = F_e \cos(\omega t)$ . As per our model approximation, we

consider the neighboring particles to have a constant displacement from equilibrium denoted by  $\Delta$ . We also assume that the defect motion happens only at the excitation frequency, and is given by  $u_d = A \cos(\omega t + \varphi)$ . We replace the particles between the defect neighbors and the walls by a linear spring with a force relation  $F(\Delta) = F_0 + K_C \Delta$ , where  $F_0$  is the static force at equilibrium and  $K_C$  is calculated by linearizing the interaction force of all the particles after the defect's neighbors and lumping them into a single spring.

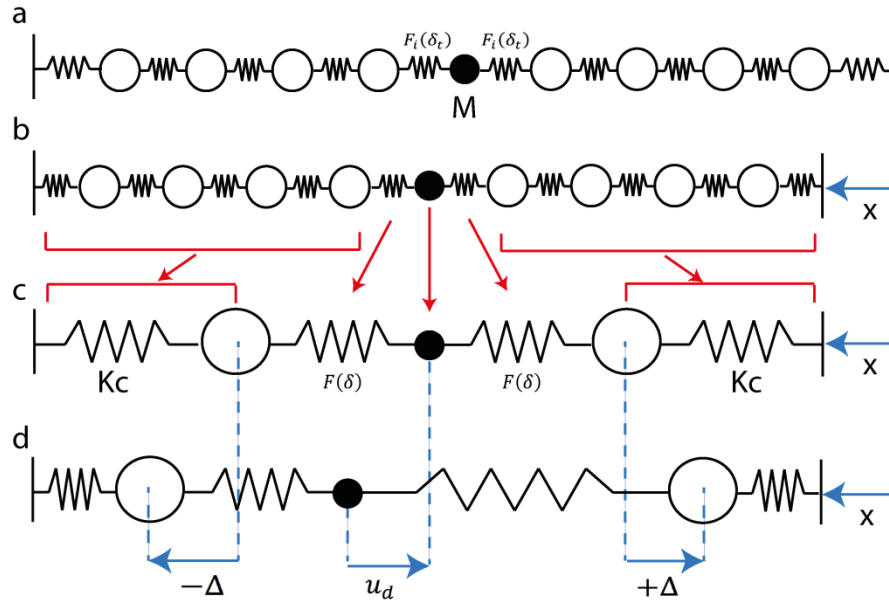


Figure A.1: Analytical modeling of the system. **a** Initial lattice with no deformation. The lattice consists of a chain of particles, where the central particle is a defect having a mass  $M$  smaller than the rest of the particles. The defect interacts with the neighbors through a nonlinear force  $F_i(\delta_t)$ , where  $\delta_t$  is the total distance separating the defect and the neighbors. **b** Deformed lattice. The lattice boundary has been displaced by an amount  $x$ . **c** Simplified system used in the analytical approximation. For each fixed displacement value  $x$ , the interaction potential between the defect and the neighbors is approximated by a third order polynomial  $F(\delta)$ , where  $\delta = \delta_t - \delta_0$ ,  $\delta_0$  being the equilibrium distance between the defect and the neighbors in the deformed lattice with no defect drive. All the other beads in the chain are approximated by two linear springs  $K_C$ , with  $K_C$  calculated independently for each deformation value  $x$ . **d** Simplified system with the defect in motion. The defect is displaced from equilibrium by an amount  $u_d$ . The two neighboring beads are

statically pushed away from it by an amount  $\Delta$  due to thermal expansion.

We further simplify the system by performing a Taylor expansion of the nonlinear spring connecting the defect mode with the two half-lattices on each side. We take the Taylor expansion up to third degree,  $F(\delta) = F_0 + k\delta + k'\delta^2 + k''\delta^3$ . Here,  $F_i(\delta_t)$  is approximated by the  $F(\delta)$ . A force including terms up to third degree is able to capture static equilibrium, linear oscillation, thermal expansion, and resonance bending effects. The expansion is calculated around the inter-particle distance at rest, denoted by  $\delta_0$ . At each deformation value, we calculate the coefficients in the Taylor expansion for the defect-neighbor interaction and the linearized spring constant for the half-lattices.

This model results in an equation of motion for the single defect particle and an equation for the static equilibrium of the defect's neighbors. Note that, due to the symmetry of the system, we only need a single equilibrium equation for the two neighbors.

$$M\ddot{u}_d + b\dot{u}_d - F(-u_d - \Delta) + F(u_d - \Delta) = F_e \cos \omega t \quad (\text{A.1})$$

$$K_C \Delta + F_0 = F(u_d - \Delta) \quad (\text{A.2})$$

To solve for the amplitude and static force, we perform a harmonic balance<sup>88</sup> including only components at the excitation frequency, and discarding terms containing powers of  $A^2$  above 3. We neglect higher frequency components because they are significantly lower in the frequency spectrum of the defect's vibration. For the neighbor's equation, we neglect all the harmonic terms and take only the zero-frequency component force. This procedure results in the following condition for the amplitude of the defect:

$$A^2 \left[ \left( 2k + \frac{3}{4} \left[ 2k'' - \frac{8}{3} \left( \frac{k'^2}{K_c + k} \right) \right] A^2 - M \omega^2 \right)^2 + (b\omega)^2 \right] - F_e^2 = 0 \quad (\text{A.3})$$

The harmonic balance condition allows us to determine the vibration amplitude of the defect, since all other variables are known: the parameters  $k$ ,  $k'$ ,  $k''$  and  $K_c$  depend on the total deformation of the lattice, which is prescribed.  $F_e$  and  $\omega$  describe the defect excitation and are also prescribed. The defect's mass  $M$  and damping  $b$  are fixed parameters of the system.

We can get further insight on the properties of this system by realizing that the amplitude condition (Eq. A.3) is identical to the one that is obtained by performing the same harmonic balance procedure on a Duffing oscillator. A Duffing oscillator is a single degree of freedom dynamical system described by the equation  $\ddot{x} + \frac{1}{\tau} \dot{x} + \omega_0^2 x + \alpha x^3 = F_d/M$ , and is an extremely well studied system. In order to transform our system into a Duffing oscillator, we use the equations:

$$\omega_0^2 = \frac{2k}{M} \quad (\text{A.4})$$

$$\alpha = \frac{1}{M} \left( 2k'' - \frac{8}{3} \frac{k'^2}{K_c} \right). \quad (\text{A.5})$$

Knowing the vibration amplitude of the defect, it is possible to determine the thermal expansion, and therefore the force at the boundary. To do so we use the defect neighbor's equilibrium equation, and the fact that the force on the linearized spring,  $K_c$ , that connects the defect's neighbors to the boundary is the same on both ends of the spring.

$$F_b = F_0 + \frac{1}{2} \left( \frac{k'}{1 + \frac{k}{k_c}} \right) A^2 \quad (\text{A.6})$$

As expected, the force at the boundary is the sum of the force without any defect drive, and a thermal expansion term that increases with increasing defect motion. The thermal expansion is a consequence of the asymmetric terms in the interaction potential. During a period of the defect oscillation around an equilibrium point, symmetric terms result in an equal amount of attractive and repulsive force. In contrast, asymmetric terms introduce different amounts of attractive and repulsive force, and therefore produce a net effect in the force at the boundary.

Since the analytical model allows us to predict the static force at each displacement value, we can differentiate this prediction with respect to the displacement in order to obtain the stiffness (Eq. A.7). This equation contains the original stiffness of the lattice, a term relating changes in force at the boundary to changes in the vibration amplitude of the defect, and a term due to the change in the thermal expansion coefficient as the lattice is compressed.

$$k = \frac{dF_b}{dx} = \frac{dF_0}{dx} + \left( \frac{k'}{1 + \frac{k}{k_c}} \right) A \frac{dA}{dx} + \frac{1}{2} A^2 \frac{d}{dx} \left( \frac{k'}{1 + \frac{k}{k_c}} \right) \quad (\text{A.7})$$

The term  $dA/dx$  can be found implicitly from the harmonic balance. This is done by thinking of the balance condition (Eq. A.3) as a function of the amplitude and displacement, and noting that the amplitude itself depends on the displacement:

$$\psi(A(x), x) = A^2 \left[ \left( 2k(x) + \frac{3}{4} \left[ 2k''(d) - \frac{8}{3} \left( \frac{k'(x)^2}{K_c(x) + k(x)} \right) \right] A^2 - M \omega^2 \right)^2 + (b\omega)^2 \right] - F_e^2. \quad (\text{A.8})$$

Since this function must stay constant at zero for all displacements, its total derivative with respect to the displacement must also be zero:

$$\frac{d\psi}{dx} = \frac{\partial\psi}{\partial A} \frac{dA}{dx} + \frac{\partial\psi}{\partial x} = 0. \quad (\text{A.9})$$

From the previous equation, it is possible to obtain a closed expression for  $dA/dx$ , provided that the amplitude of oscillation is known:

$$\frac{dA}{dx} = - \frac{\left( \frac{\partial\psi}{\partial x} \right)_A}{\left( \frac{\partial\psi}{\partial A} \right)_x}. \quad (\text{A.10})$$

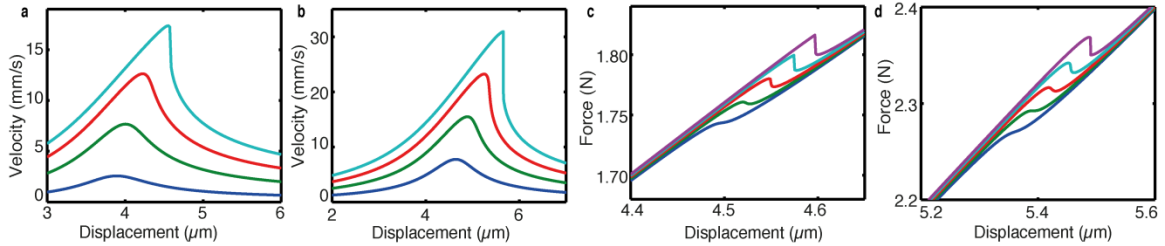


Figure A.2: Analytical predictions and comparison to numerical results. **a** Defect response obtained by numerically integrating the equations of motion for the full system. **b** Defect response predicted by the analytical model **c** Force- displacement relation of the material obtained through numerical integration **d** Force- displacement relation obtained analytically. All panels are calculated for an excitation frequency of 10.5 KHz at increasing excitation amplitudes.

We have created a simplified model that captures the tuning of the incremental stiffness through the excitation of local defect modes. We use the model to engineer the nonlinear interaction potential so it allows us to tune the stiffness to arbitrarily positive values. This is accomplished by looking at the stiffness equation (Eq. A.7). When the changes in the stiffness are very large, the term  $k'A \partial A / \partial x$  is always dominant. This is because  $\partial A / \partial x$  can grow arbitrarily large, while the other terms in the equation are bounded. The term's contribution to the stiffness of the chain,  $K$ , is given by:

$$\Delta K = - \frac{A}{1 + \frac{k}{K_c}} \frac{k' \left( \frac{\partial \psi}{\partial x} \right)_A}{\left( \frac{\partial \psi}{\partial A} \right)_x}. \quad (\text{A.11})$$

This contribution is large when the system approaches a bifurcation. When that happens,  $\partial \psi / \partial x$  tends to zero. Depending on the sign of the numerator  $-k'(\partial \psi / \partial x)$ , the stiffness will grow arbitrarily positive or arbitrarily negative. We study this value for a power law potential,  $F = Ax^p$  (Fig. A.3a). When the exponent  $p$  is between 0 and 1, the numerator is positive. In lattices with this kind of interaction force law, the stiffness can be tuned to arbitrarily positive values (Figs. A.3b and A.3c). Recently proposed theoretical work<sup>S141</sup> combined with novel microfabrication techniques<sup>S142</sup> should enable the design of mechanical lattices with tailored interaction potentials. Therefore, it should be possible to create materials with stiffness that can be tuned over a broad range to positive or negative values.

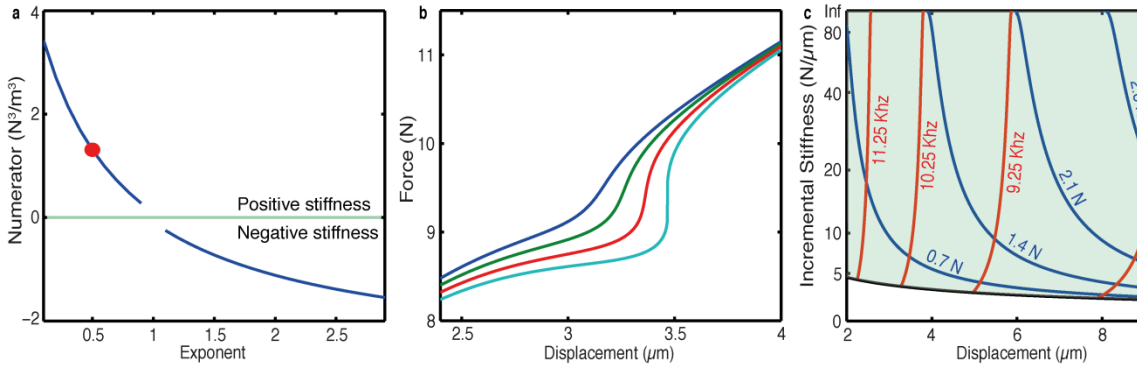


Figure A.3: Stiffness tuning to positive infinity. **a** Stiffness numerator corresponding to a power law potential  $F = \frac{1}{p} \delta_t^p$  as a function of the exponent. Calculated for a chain of 9 particles with  $\delta_T = 1$ . Parameters are  $M = 1$  and  $b = 0.025$ . **b** Force-displacement curves for a 9-particle lattice with a power law interaction force exponent  $F = Ap^{0.5}$ ,  $A = 5600$ . The exponent 0.5 is indicated as a red dot in **a**. The curves correspond to an excitation frequency of 10.5 KHz and increasing excitation forces. **c** Map relating the applied excitation frequency and amplitude to the stiffness, for the same system as **b**. In all panels the interaction force law is assumed to be equal between all neighboring particles. For **b** and **c**, the defect's mass and damping are the same as in Fig A.2.

## 1.2 Analysis for strongly nonlinear frequency bands

This section follows the experimental results from chapter 8. The analysis examines the extension from a system of two beads to frequency bands in the infinite limit. This analysis was done principally by K.R. Jayaprakash.

In this section, we analytically study the weakly nonlinear dynamics in the AB (attenuation band). The induced permanent compression leads to a linearizable system suitable for analytical techniques. We extend the previous results by considering a homogeneous crystal of  $N$  beads. Similar to the setup explained in section 3.34 for two beads, the first bead is harmonically driven and the  $N$ -th bead is constrained by a fixed wall. All the beads interact with their nearest neighbors through Hertzian interaction law. We incorporate linear viscous damping (coefficient  $\lambda$ ) between interacting beads to simulate dissipative effects in the

experimental system and to suppress transient dynamics. Here, we account for the damping force only when the beads are in contact and thus incorporate the Heaviside function ( $\Theta$ ) on the relative displacement of the beads. In our analytical approach we non-dimensionalize the equations of motion so that the results are of general applicability. We therefore begin with presenting the equations of motion of the theoretical model of an  $N$  bead chain with right end fixed and the left end harmonically excited:

$$\begin{aligned}
m_1 \frac{d^2 u_1}{dt^2} &= (4/3)E_{1*} \sqrt{R} (F(t) - u_1)_+^{3/2} - (4/3)E_* \sqrt{\frac{R}{2}} (u_1 - u_2)_+^{3/2} + \\
&\quad \lambda (\dot{f}(t) - \dot{u}_1) \Theta [f(t) - u_1] - \lambda (\dot{u}_1 - \dot{u}_2) \Theta [u_1 - u_2] \\
&\quad \dots \\
m_i \frac{d^2 u_i}{dt^2} &= (4/3)E_* \sqrt{\frac{R}{2}} \left\{ (u_{i-1} - u_i)_+^{3/2} - (u_i - u_{i+1})_+^{3/2} \right\} + \\
&\quad \lambda (\dot{u}_{i-1} - \dot{u}_i) \Theta [u_{i-1} - u_i] - \lambda (\dot{u}_i - \dot{u}_{i+1}) \Theta [u_i - u_{i+1}] \\
&\quad \dots \\
m_N \frac{d^2 u_N}{dt^2} &= (4/3)E_* \sqrt{\frac{R}{2}} (u_{N-1} - u_N)_+^{3/2} - (4/3)E_{2*} \sqrt{R} (u_N)_+^{3/2} + \\
&\quad \lambda (\dot{u}_{N-1} - \dot{u}_N) \Theta [u_{N-1} - u_N] - \lambda (\dot{u}_N) \Theta [u_N],
\end{aligned} \tag{A.12}$$

where  $i = 2, 3, \dots, (N-1)$  are the bead subscripts and  $F(t) = A \sin(\omega t)$  is the harmonic base excitation. The appropriate non-dimensionalization leads to the set of normalized equations of motion,

$$\begin{aligned}
\frac{d^2 X_1}{d\tau^2} &= \eta [\sin(\beta\tau) - X_1]_+^{3/2} - \frac{1}{\sqrt{2}} (X_1 - X_2)_+^{3/2} + \\
&\xi (\beta \cos(\beta\tau) - X'_1) \Theta [\sin(\beta\tau) - X_1] - \xi (X'_1 - X'_2) \Theta [X_1 - X_2] \\
&\quad \dots \\
\frac{d^2 X_i}{d\tau^2} &= \frac{1}{\sqrt{2}} \{ (X_{i-1} - X_i)_+^{3/2} - (X_i - X_{i+1})_+^{3/2} \} + \\
&\xi (X'_{i-1} - X'_i) \Theta [X_{i-1} - X_i] - \xi (X'_i - X'_{i+1}) \Theta [X_i - X_{i+1}] \\
&\quad \dots \\
\frac{d^2 X_N}{d\tau^2} &= \frac{1}{\sqrt{2}} (X_{N-1} - X_N)_+^{3/2} - \alpha (X_N)_+^{3/2} + \\
&\xi (X'_{N-1} - X'_N) \Theta [X_{N-1} - X_N] - \xi (X'_N) \Theta [X_N],
\end{aligned} \tag{A.13}$$

where  $E_*$  is the effective stiffness between the interacting beads, and  $X_i = u_i / A$ ,  $\tau = (4E_* \sqrt{AR} / 3m)^{1/2} t \equiv \psi t$ ,  $\eta = E_{1*} / E_*$ ,  $\alpha = E_{2*} / E_*$ ,  $\beta = \omega / \psi$ , and  $\xi = \lambda / m\psi$  are non-dimensional variables relating (3) and (4). Without loss of generality, we consider  $\eta = 1$  and  $\alpha = 1$  denoting that the dynamic sensor, actuator, and beads are made of the same material. This does not affect the validity of the resulting dynamics. Recalling the material and experimental data from section 3.3.4, we obtain  $E_* = E_s / [2(1 - \nu_s^2)]$ ,  $A = 3.5 \times 10^{-7} m$ , and  $\omega = 8500 \text{ Hz}$ ; moreover, the non-dimensional quantities are computed as  $\beta = 3.1742$ ,  $\psi = 1.6825 \times 10^4$ , and  $\xi = 0.5$ .

As a second step, and in view of the fact that a sustained compression is experienced by the beads in the AB, we decompose the bead displacements into ‘static’ (permanent constant compression) and ‘dynamic’ (oscillatory) components. For high frequency excitations in the AB, experiment and simulation indicate that small amplitude oscillations about a permanent compressed state occur, and this decomposition is in line with this observation. This motivates

us to introduce new translated coordinates  $X_j(\tau) = \delta_j + x_j(\tau)$ , where the  $j$ -th bead's displacement is expressed as a combination of its static,  $\delta_j > 0$ , and dynamic,  $x_j(t)$ , components. In simulations we observed that  $\delta_j > \delta_{j+1}$ , i.e., that the permanent compression experienced by each bead decreases as we move away from the actuator and the standing wave oscillation in the AB becomes spatially localized (Fig. A.4). The axes in Fig. A4-A8 denote the non-dimensional units derived above. From the previously shown results it can be deduced that no separation occurs between beads once the dynamics enters the AB, i.e., the dynamics is smooth between interacting beads. Therefore the subscript '+' can be eliminated from the equations of motion (Eq. A.13), which greatly facilitates the asymptotic analysis. The only exception is the contact between the actuator and first bead.

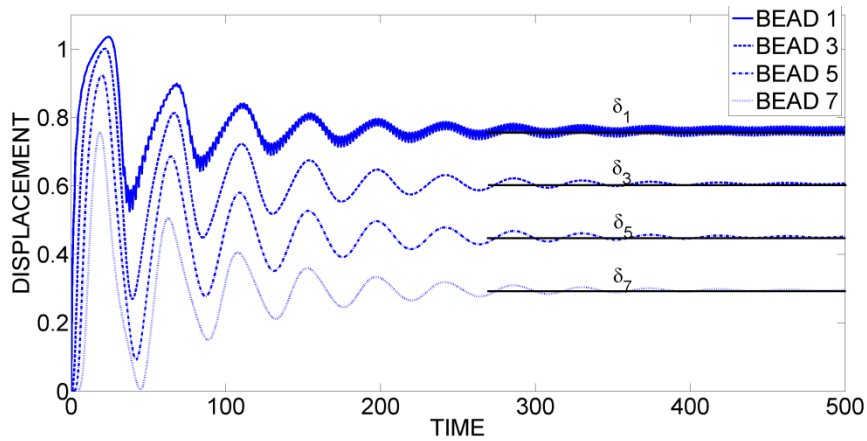


Figure. A.4: The displacement response of 1<sup>st</sup>, 3<sup>rd</sup>, 5<sup>th</sup>, and 7<sup>th</sup> beads of a 10 bead homogeneous chain under harmonic excitation with frequency in the attenuation zone. All units are non-dimensional.

When the dynamics is well inside the AB it holds that  $|\sin(\beta\tau) - \delta_1| \gg x_1(\tau)$ , except in the close neighborhood of points ‘a’ and ‘b’ as shown in Fig. A.5a. Thus, it can be assumed that  $[\sin(\beta\tau) - \delta_1 - x_1] > 0$  in the region between points ‘a’ and ‘b’ where the actuator displacement exceeds the permanent compression of the first bead  $\delta_1$ , and  $[\sin(\beta\tau) - \delta_1 - x_1] < 0$  when the actuator displacement is less than  $\delta_1$ .

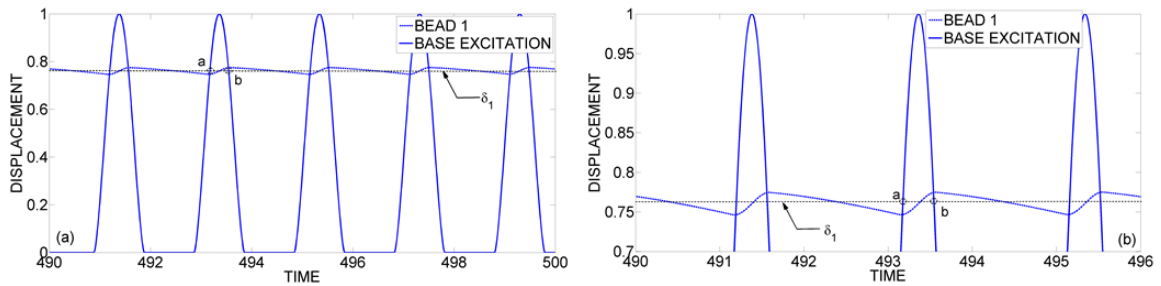


Figure A.5: The displacement response of the 10-bead homogeneous chain under harmonic excitation with frequency in the attenuation zone: (a) Response of the first bead superimposed to the excitation, and (b) detail of (a). All units are non-dimensional.

Figure A.5b shows a detailed view of the region between points ‘a’ and ‘b’. It follows that we can modify (4) by decomposing the responses in terms of static and dynamic components and incorporating the observations mentioned above. This leads to the following modified equations:

$$\begin{aligned} \frac{d^2 x_1}{d\tau^2} = & \eta [\sin(\beta\tau) - \delta_1]_+^{3/2} - \frac{3}{2} \eta [\sin(\beta\tau) - \delta_1]_+^{1/2} x_1 - \\ & \frac{1}{\sqrt{2}} (\delta_1 - \delta_2)^{3/2} - \frac{3}{2\sqrt{2}} (\delta_1 - \delta_2)^{1/2} (x_1 - x_2) + \\ & \xi(\beta \cos(\beta\tau) - x'_1) H[\sin(\beta\tau) - \delta_1] - \xi(x'_1 - x'_2) + O(x_1^p x_2^q) \\ & \dots \end{aligned}$$

$$\frac{d^2 x_i}{d\tau^2} = \frac{1}{\sqrt{2}} \left\{ (\delta_{i-1} - \delta_i)^{3/2} + \frac{3}{2} (\delta_{i-1} - \delta_i)^{1/2} (x_{i-1} - x_i) - (\delta_i - \delta_{i+1})^{3/2} - \frac{3}{2} (\delta_i - \delta_{i+1})^{1/2} (x_i - x_{i+1}) \right\}_+ + \xi(x'_{i-1} - 2x'_i + x'_{i+1}) + O(x_{i-1}^p x_i^q) + O(x_i^r x_{i+1}^s)$$

...

$$\begin{aligned} \frac{d^2 x_N}{d\tau^2} = & \frac{1}{\sqrt{2}} (\delta_{N-1} - \delta_N)^{3/2} + \frac{3}{2\sqrt{2}} (\delta_{N-1} - \delta_N)^{1/2} (x_{N-1} - x_N) - \alpha (\delta_N)^{3/2} - \frac{3}{2} \alpha (\delta_N)^{1/2} x_N \\ & + \xi(x'_{N-1} - 2x'_N) + O(x_{N-1}^p x_N^q) + O(x_N^z) \end{aligned}$$

$$i = 2, 3, \dots, (N-1), \quad p+q \geq 2, \quad r+s \geq 2, \quad z \geq 2.$$

As in the previous discussion, the only non-smooth component is in the first equation of (Eq. A.14), modeling the separation of the actuator and first bead.

We observe that there are two terms on the right hand side of (Eq. A.14) resulting from the interaction between beads; namely static components dependent only on  $\delta_j$ , and dynamic components involving  $x_j(\tau)$ . We account for the non-smooth terms in (Eq. A.14) by expanding the harmonic excitation term  $\left([\sin(\beta\tau) - \delta_1]_+^{3/2}\right)$  in Fourier series to obtain ‘static’ and ‘dynamic’ components as follows:

$$[\sin(\beta\tau) - \delta_1]_+^{3/2} = a_0 + \sum_{n=1}^{\infty} a_n \cos(n\beta\tau) + \sum_{n=1}^{\infty} b_n \sin(n\beta\tau) \quad (\text{A.15})$$

with the coefficients defined as:

$$\begin{aligned} a_0 &= \frac{\beta}{2\pi} \int_{-\pi/\beta}^{\pi/\beta} [\sin(\beta\tau) - \delta_1]_+^{3/2} d\tau \\ a_n &= \frac{\beta}{\pi} \int_{-\pi/\beta}^{\pi/\beta} [\sin(\beta\tau) - \delta_1]_+^{3/2} \cos(n\beta\tau) d\tau \\ b_n &= \frac{\beta}{\pi} \int_{-\pi/\beta}^{\pi/\beta} [\sin(\beta\tau) - \delta_1]_+^{3/2} \sin(n\beta\tau) d\tau. \end{aligned} \quad (\text{A.16})$$

Now, by balancing the static components in all (smooth) equations (Eq. A.14), we obtain the following recursive relation that can be used for computing the permanent compression between beads:

$$\begin{aligned} (\delta_{j-1} - \delta_j)^{3/2} - (\delta_j - \delta_{j+1})^{3/2} &= 0 \\ \dots & \\ \frac{1}{\sqrt{2}}(\delta_{N-1} - \delta_N)^{3/2} - \alpha(\delta_N)^{3/2} &= 0. \end{aligned} \quad (\text{A.17})$$

where  $j = 2, 3, \dots, (N-1)$ . A trivial algebraic manipulation yields,

$$\delta_{j-1} = 2\delta_j - \delta_{j+1} \quad (\text{A.18})$$

$$\begin{aligned} \dots & \\ \delta_{N-1} &= \delta_N(1 + \gamma) \end{aligned} \quad (\text{A.19})$$

$$\delta_i = \frac{\delta_{i-1} [1 + (N-i)\gamma]}{[1 + (N-i+1)\gamma]}, \quad 1 < i \leq N,$$

where  $\gamma = 2^{1/3} \alpha^{2/3}$ . The only unknown in the above set of equations is the permanent compression of the first bead,  $\delta_1$ . Once this is evaluated the compression of all the other beads can be expressed in terms of  $\delta_1$ . The compression  $\delta_1$  can be obtained by balancing the static force components in the first equation of (Eq. A.14), i.e., balancing the constant term from the Fourier series (Eq. A.15) with the constant force interaction between the first and the second beads. Then, we obtain an implicit relation of the form,

$$\frac{\eta\beta}{2\pi} \int_{-\pi/\beta}^{\pi/\beta} [\sin(\beta\tau) - \delta_1]_+^{3/2} d\tau - \frac{1}{\sqrt{2}} (\delta_1 - \delta_2)^{3/2} = 0. \quad (\text{A.20})$$

Substituting for  $\delta_2$  in terms of  $\delta_1$  and rescaling time  $\tilde{\tau} = \beta\tau$ , we derive the final form for the equation governing the permanent compression of the first bead,

$$\left\{ \frac{\eta}{\pi} \int_{\sin^{-1}(\delta_1)}^{\pi/2} (\sin(\tilde{\tau}) - \delta_1)^{3/2} d\tilde{\tau} \right\}^{2/3} = \delta_1 \left[ \frac{1}{1 + (N-1)\gamma} \right], \quad (\text{A.21})$$

where the '+' sign is removed from (Eq. A.19) since  $(\sin(\tilde{\tau}) - \delta_1)^{3/2} \geq 0$  within the limits of integration.

The above equation is evaluated numerically to obtain  $\delta_1$ . This analysis predicts that the static compression  $\delta_1$  of the first bead (and therefore of any other bead) is independent of the

excitation frequency when the dynamics is well inside the AB (i.e., for relatively high frequencies). This is verified through numerical simulations (Fig. A.6), where we depict the response of the first bead for a homogeneous chain with  $N=10$  at various excitation frequencies  $\beta$  inside the AB. The static component of the response is independent of the excitation frequency. This analysis assumes weakly nonlinear behavior, and these predictions are not valid at lower frequencies as the dynamics makes the transition from the PB (propagation band) to the AB (attenuation band).

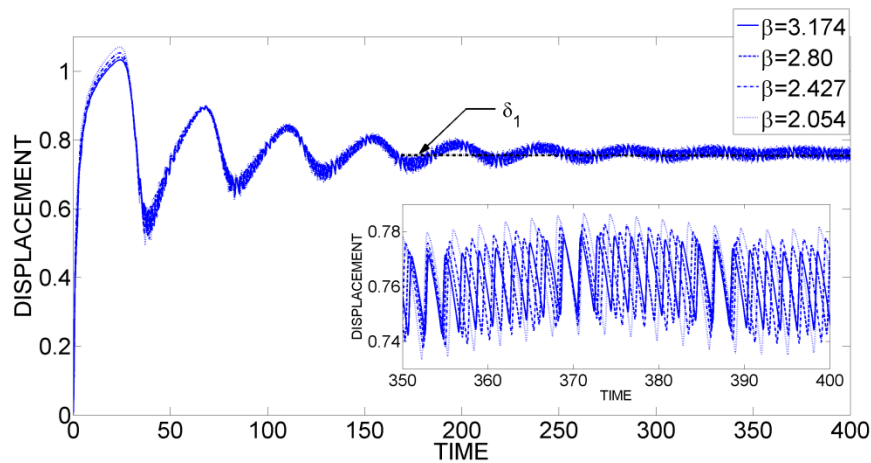


Figure A.6 (Color online) the displacement response of first bead of a 10-bead homogeneous chain with varying normalized excitation frequency and fixed normalized excitation amplitude equaling unity (dynamics deep inside the attenuation zone). All units are non-dimensional.

The static overlap of each bead in the granular chain is evaluated using (Eq. A.18, A.19, and A.20) and is compared to the results derived from numerical simulation for a 20 bead crystal,  $N=20$  (Fig. A.7). The numerical simulations show good correspondence with the analytical estimates and confirm that the spatial variation of the static overlap is nearly linear. As the length of the crystal is increased the static component of the first bead's displacement reaches

unity asymptotically, whereas the static offset of the last bead approaches zero. Hence, the resulting standing wave oscillations executed by the beads become spatially localized well inside the AB of the harmonically forced system. In essence, for a sufficiently large number of beads, the chain detaches from the exciter and the energy input to the chain approaches zero asymptotically.

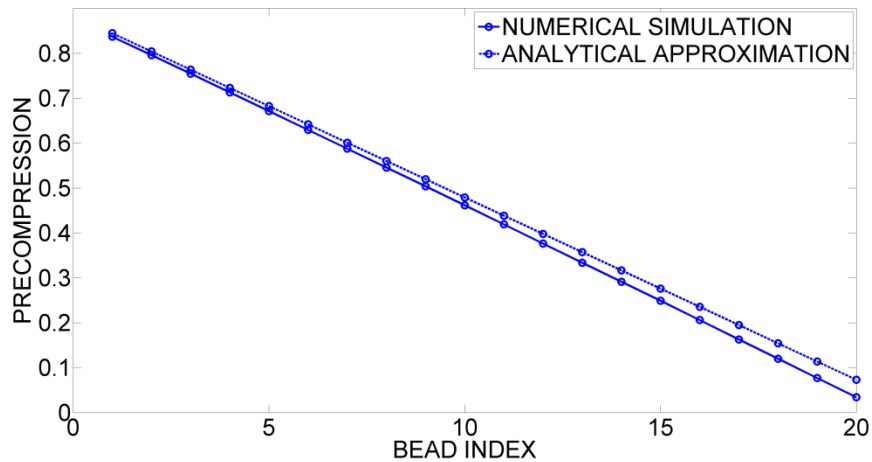


Figure A.7: Spatial variation of permanent precompression ( $\delta_i$ ) in a 20 bead chain when the dynamics is deep in the attenuation zone. All units are non-dimensional.

Finally, we obtain analytic estimates of the individual oscillatory responses of the beads by considering the dynamic components of the bead displacements in (Eq. A.14). We arrive at reduced dynamic equations for each  $x_j(\tau)$  by removing the static components of (Eq. A.14). These reduced equations depend on the dynamic components of the Fourier series expansion (Eq. A.15). We then find analytic approximations for the oscillatory components of the bead responses for an  $N$  degree of freedom linear damped oscillator system with periodically varying forcing frequency. The presence of damping terms leads to steady state periodic responses. Due to the presence of damping, the amplitudes of the dynamic components of the

bead responses (i.e., the oscillations about the beads' static offsets) decrease with increasing frequency. For a particular fixed frequency these amplitudes decrease away from the site of the actuator, i.e.,  $x_j(\tau) > x_{j+1}(\tau)$ , confirming the attenuatory nature of the dynamics, as described above.

The agreement between numerical and analytical response for the forced two-bead system is presented in Fig. A.8. The analytical responses closely match the numerical ones, and both  $x_1(\tau) > x_2(\tau)$  and  $\delta_1 > \delta_2$ . Although the transient dynamics is not captured by our analytic study, the steady state dynamics shows good correspondence between analytical prediction and numerical simulation.

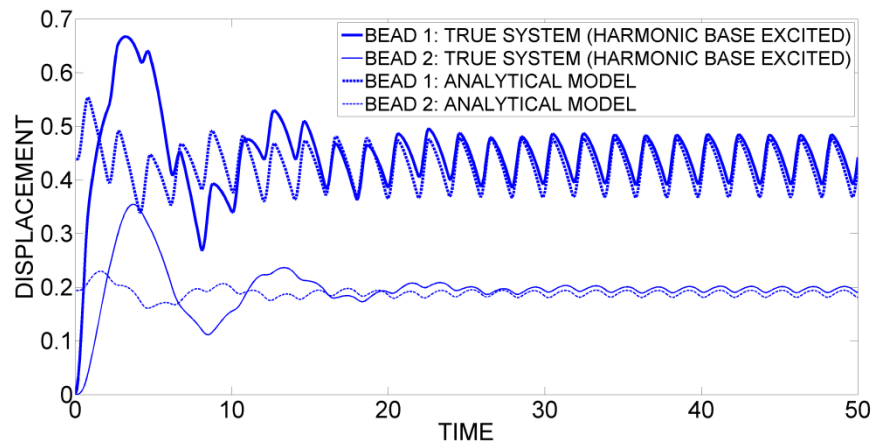


Figure A.8: Correspondence between analytical and numerical response of the 2-bead system when the dynamics is in the attenuation zone. All units are non-dimensional.